# Lattice Dynamics of Metal-Organic Frameworks (MOFs): Neutron Inelastic Scattering and First-Principles Calculations

W. Zhou[1,2] and T. Yildirim[1,2]
[1]*NIST Center for Neutron Research, National Institute of Standards and Technology, Gaithersburg, Maryland 20899, USA*
[2]*Department of Materials Science and Engineering, University of Pennsylvania, Philadelphia, Pennsylvania 19104, USA*

(Dated: February 6, 2008)

By combining neutron inelastic scattering (NIS) and first-principles calculations, we have investigated the lattice dynamics of MOF5. The structural stability of MOF5 was evaluated by calculating the three cubic elastic constants. We find that the shear modulus, $c_{44}$ = 1.16 GPA, is unusually small, while two other moduli are relatively large (i.e. $c_{11}$ = 29.42 GPa and $c_{12}$ = 12.56 GPa). We predict that MOF5 is very close to structural instability and may yield interesting new phases under high pressure and strain. The phonon dispersion curves and phonon density of states were directly calculated and our simulated NIS spectrum agrees very well with our experimental data. Several interesting phonon modes are discussed, including the softest twisting modes of the organic linker.

PACS numbers: 63.20.-e, 62.20.Dc, 61.82.Pv



Metal-organic framework (MOF) compounds,[1,2,3,4] which consist of metal-oxide clusters connected by organic linkers (see Fig. 1), are a new class of nanoporous materials with very promising potential applications such as energy storage, gas separation, and template synthesis of nanoclusters and catalysts. There are an almost exponentially growing number of studies on MOF materials, mostly focusing on the optimization of the metal-oxide clusters and/or the organic linkers to improve the gas adsorption properties. Much less attention is paid to the fundamental properties of this interesting class of materials such as their structural stability and lattice dynamics. Understanding the stability and dynamical properties is clearly needed in order to optimize these materials for desired properties. For example, it was recently proposed that the MOF structure can encapsulate $C_{60}$ molecules and result in superconductivity upon doping[5]. In such hybrid structures, it is important to know the phonon spectrum of the MOF lattice and its coupling to the electronic structure. Furthermore, a lack of knowledge concerning MOFs lattice dynamics presents a significant obstacle in the quantum dynamics study of gas molecules ($H_2$, $CH_4$ etc.) adsorbed on MOFs[6,7].

Here we report a detailed study of the structural stability and lattice dynamics of MOF5 (the most widely studied MOF material) from combined neutron inelastic scattering (NIS) and first-principles calculations. The structure of MOF5 (Fig.1) is highly symmetric (space group *Fm-3m*) and consists of $ZnO_4$ clusters at the tetrahedral site of an *fcc* lattice, linked by 1,4-benzenedicarboxylate (BDC) to form the three dimensional framework.

Our first-principles calculations were performed within the plane-wave implementation of the local density approximation to density functional theory in the PWscf package[8]. We used Vanderbilt-type ultrasoft potentials with Perdew-Zunger exchange correlation. A cutoff energy of 408 eV and a 1×1×1 k-point mesh were found to be enough for the total energy to converge within 0.5meV/atom.

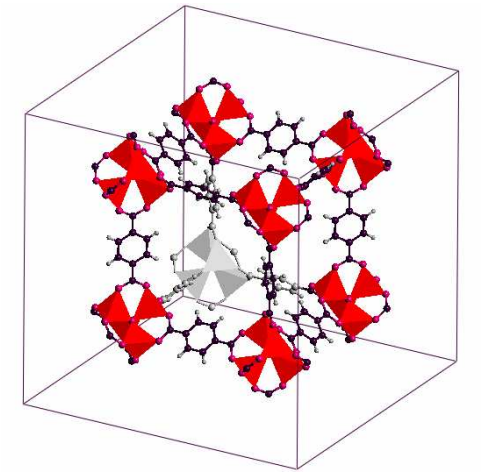

FIG. 1: (Color online) The crystal stucture of MOF5, which consists of BDC-linkers connecting $ZnO_4$ clusters located at the tetrahedral site of an fcc lattice. For clarity, some of the atoms were not shown.

We first describe the dependence of the structure on the cell volume (i.e. external pressure). Figure 2 shows how the lattice parameter and the total energy of the cell changes with external pressure and the total volume, respectively. We optimized the atomic positions for each volume and did not find any structural instability over the pressure range studied. From -0.5 to 0.5 GPa, we find a linear pressure dependence of the lattice constant with a slope of 0.46 Å/GPa. Fitting the energy vs. volume curve to the Murnaghan equation of state[9] yields a bulk modulus of 18.2 GPa. The minimum energy corresponds to lattice constant $a_C$ = 25.58 Å, which is in excellent agreement with the experimental value[10] of $a$ = 25.91 Å. The optimized atomic positions were also found to agree well with the experimental values.

A better insight into the structural stability can be gained from the elastic constants, which we calculated

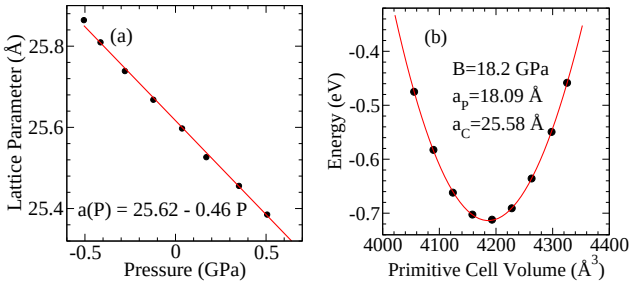


FIG. 2: (Color online) Left: The cubic lattice parameter of MOF5 versus pressure, indicating linear dependence near equilibrium structure. Right: The total energy versus primitive cell volume (dots) and the fit by Murnaghan equation of state (solid line).

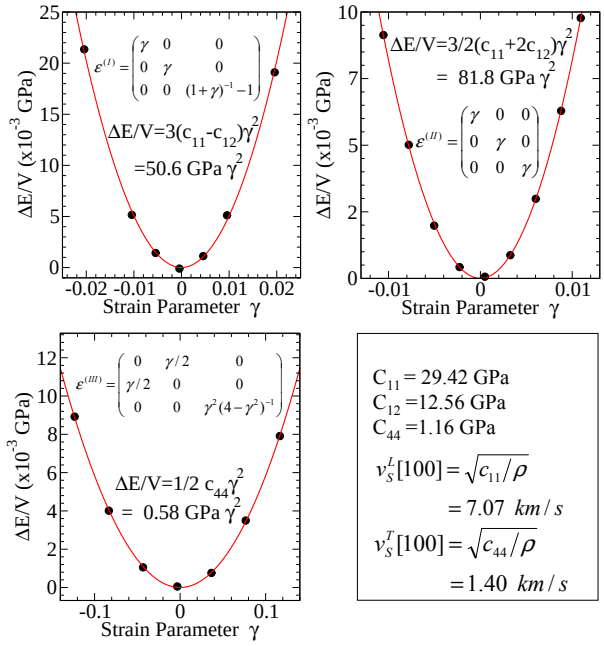


FIG. 3: (Color online) The three cubic elastic constants of MOF5. The dots are the actual calculations and the solid lines are the quadratic fit. The deformation matrices for each distortion are also shown. The right-bottom panel summarizes the calculated elastic moduli and the sound-velocities. Here $\rho$ is the mass density of MOF5 (0.59 g/cm$^3$).

following the standard scheme for a cubic crystal[11,12], starting from the fully optimized MOF5 structure. Three types of strains were applied to the conventional fcc cell of MOF5 (see Fig. 3). Strain *I* is a stretch along the z axis; strain *II* is a monoclinic shear about the *z* axis. Both strain *I* and *II* are volume-conserving. Strain *III* simply changes the lattice constant *a*. For all three strains, there is only one variable, $\gamma$, in the strain tensor, reflecting the magnitude of the strain. All calculations were done on the strained primitive cell, which is structurally equivalent to the strained conventional cell. Atomic positions were fully optimized and $E$ vs. $\gamma$ data were obtained. $E(\gamma)/V$ was then fit to a polynomial in $\gamma$, where $V$ is the unit cell volume. The results are summarized in Fig. 3. As expected, the calculated elastic constants satisfy the stability criteria (i.e. $c_{11} > c_{12}$, $c_{11} + 2c_{12} > 0$, and $c_{44} > 0$ for a cubic crystal). However, the shear modulus $c_{44}$ is very small (1.16 GPa), indicating that MOF5 is very close to structural instability. Besides, $c_{11} - c_{44}$ is significantly larger than zero and according to the Cauchy relation[13], this indicates a significant deviation from a central intermolecular potential. The small $c_{44}$ also suggests that MOF5 could collapse into a potentially useful structure under certain shear-stress. For examples, the pristine MOF5 structure has a large pore volume but the pores are too open to hold hydrogen molecules at high temperatures; a collapsed MOF5 structure could have finer cavities connected by smaller channels, which are in principle better for $H_2$ storage.

After having shown that the MOF5 structure is stable with a very small shear modulus, we now discuss the lattice dynamics properties at the zone center and along high-symmetry directions in the Brillouin zone. The phonon density of states (DOS) and dispersion curves were calculated using the supercell method with finite difference.[14] The primitive cell was used and the full dynamical matrix was obtained from a total of 26 symmetry-independent atomic displacements (0.03 Å).

The primitive cell of MOF5 contains two formula units ($Zn_4O_{13}$-$(C_8H_4)_3$) giving rise to a total of 318 phonon branches. The phonon modes at Γ are classified as

$$\Gamma\ (q{=}0) = 9A_{1g}(R) + 3A_{1u} + 3A_{2g} + 9A_{2u} + 12E_u + 12E_g(R) + 17T_{2u} + 24T_{2g}(R) + 24T_{1u}(IR) + 17T_{1g}$$

where R and IR correspond to Raman- and infrared-active, respectively. The crystal symmetry implies 105 Raman- and 72 IR-active modes. In Table I, we list the calculated energies at Γ. We hope that our calculations will initiate more experimental work such as Raman/IR measurements to confirm the gamma phonon energies that we calculated here. In the absent of such high-resolution data, we have performed neutron inelastic scattering measurements of the phonon DOS and compared it with our calculations.

The experimental NIS spectrum shown in Fig.4 was collected on a powder sample of MOF5 using the Filter Analyzer Neutron Spectrometer[15] (FANS) under conditions that provide full-width-at-half-maximum energy resolutions of 2-4.5% of the incident energy over the range probed. To compare the NIS data with theory, the NIS spectrum was computed for a 10×10×10 q-point grid within the incoherent approximation[14,16], with instrumental resolution taken into account. As shown in Fig. 4, the agreement between calculation and experiment is excellent. In contrast to Raman and IR spectroscopy, neutron spectroscopy is not subject to any selection rules, thus all modes falling in the energy range covered by our measurement (∼20 to 170 meV) were detected. Within this $E$ range, the NIS spectrum is dominated by one-phonon processes. The two-phonon contribution coming from the combination of one-phonon processes is not sig-

TABLE I: List of phonon symmetries and calculated energies (in meV) of MOF5 at the Γ point of the primitive cell.

| | | | | | | | | | |
|---|---|---|---|---|---|---|---|---|---|
| $A_{2g}$ | 2.6 | $A_{2u}$ | 23.7 | $3T_{1g}$ | 74.3 | $A_{1u}$ | 121.0 | $2E_g$ | 171.0 |
| $3T_{1g}$ | 3.1 | $A_{1g}$ | 28.7 | $3T_{2g}$ | 74.6 | $3T_{2u}$ | 121.0 | $3T_{2g}$ | 171.3 |
| $2E_g$ | 3.5 | $3T_{1u}$ | 31.7 | $3T_{1g}$ | 75.4 | $2E_u$ | 121.1 | $A_{1g}$ | 171.9 |
| $3T_{2u}$ | 3.7 | $3T_{2u}$ | 32.5 | $3T_{2g}$ | 75.8 | $2E_u$ | 124.8 | $3T_{1g}$ | 183.0 |
| $3T_{2u}$ | 5.3 | $3T_{1g}$ | 33.3 | $2E_g$ | 81.9 | $3T_{1u}$ | 124.9 | $2E_u$ | 183.5 |
| $3T_{1u}$ | 6.8 | $A_{2u}$ | 33.7 | $3T_{2g}$ | 82.1 | $A_{2u}$ | 124.9 | $3T_{1u}$ | 183.5 |
| $2E_u$ | 8.0 | $3T_{1u}$ | 34.2 | $3T_{1g}$ | 82.1 | $3T_{2u}$ | 131.7 | $A_{2u}$ | 183.5 |
| $3T_{1g}$ | 9.5 | $3T_{2g}$ | 34.3 | $3T_{2g}$ | 82.2 | $3T_{1u}$ | 131.7 | $3T_{2g}$ | 183.6 |
| $A_{1u}$ | 10.1 | $2E_u$ | 34.6 | $A_{1g}$ | 82.7 | $2E_g$ | 137.1 | $2E_g$ | 190.6 |
| $A_{2g}$ | 10.8 | $3T_{2g}$ | 43.0 | $3T_{2u}$ | 88.8 | $3T_{2g}$ | 137.2 | $3T_{2g}$ | 190.7 |
| $3T_{2g}$ | 10.9 | $3T_{1g}$ | 43.5 | $3T_{1u}$ | 89.2 | $A_{1g}$ | 137.2 | $A_{1g}$ | 191.1 |
| $3T_{1g}$ | 11.0 | $A_{1u}$ | 49.0 | $2E_u$ | 95.7 | $2E_g$ | 140.4 | $3T_{2u}$ | 191.6 |
| $3T_{2g}$ | 13.5 | $3T_{2u}$ | 49.1 | $3T_{1u}$ | 96.3 | $2E_u$ | 140.6 | $3T_{1g}$ | 193.5 |
| $3T_{2u}$ | 13.6 | $2E_u$ | 49.1 | $A_{2u}$ | 97.5 | $3T_{2g}$ | 140.6 | $3T_{1u}$ | 196.2 |
| $3T_{1u}$ | 14.2 | $3T_{2g}$ | 54.5 | $3T_{1g}$ | 98.3 | $3T_{1u}$ | 140.6 | $3T_{2g}$ | 197.5 |
| $2E_g$ | 15.2 | $A_{1g}$ | 55.3 | $3T_{2g}$ | 98.5 | $A_{2u}$ | 140.8 | $2E_u$ | 381.6 |
| $3T_{1g}$ | 15.7 | $2E_g$ | 55.9 | $2E_g$ | 102.3 | $A_{1g}$ | 141.2 | $3T_{1u}$ | 381.6 |
| $3T_{1u}$ | 16.1 | $3T_{2u}$ | 56.1 | $3T_{2g}$ | 102.6 | $3T_{1g}$ | 154.3 | $A_{2u}$ | 381.6 |
| $3T_{2u}$ | 17.4 | $3T_{1u}$ | 56.1 | $A_{2g}$ | 103.0 | $3T_{2g}$ | 154.3 | $3T_{1g}$ | 381.7 |
| $2E_u$ | 18.5 | $3T_{1u}$ | 57.8 | $A_{1g}$ | 103.2 | $2E_u$ | 167.9 | $3T_{2g}$ | 381.7 |
| $3T_{2g}$ | 18.5 | $3T_{2g}$ | 59.0 | $3T_{1g}$ | 103.2 | $3T_{1u}$ | 168.1 | $3T_{2u}$ | 383.0 |
| $3T_{1g}$ | 18.9 | $A_{2u}$ | 68.2 | $2E_g$ | 103.3 | $A_{2u}$ | 169.0 | $3T_{1u}$ | 383.0 |
| $3T_{2u}$ | 19.7 | $2E_u$ | 68.6 | $3T_{2u}$ | 107.7 | $3T_{2u}$ | 170.1 | $2E_g$ | 383.2 |
| $3T_{2g}$ | 20.6 | $3T_{1u}$ | 68.6 | $3T_{1u}$ | 107.8 | $3T_{1u}$ | 170.2 | $3T_{2g}$ | 383.2 |
| $2E_g$ | 21.5 | $3T_{2u}$ | 72.5 | $3T_{1g}$ | 119.5 | $3T_{2u}$ | 171.0 | $A_{1g}$ | 383.3 |
| $3T_{1u}$ | 22.0 | $3T_{1u}$ | 73.1 | $3T_{2g}$ | 119.6 | $3T_{1u}$ | 171.0 | | |

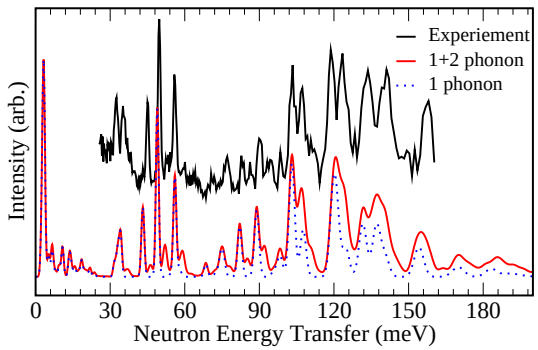


FIG. 4: (Color online) Measured NIS spectrum of MOF5 at 4 K (top curve) along with calculated spectrum (bottom curves). The calculated 1 (dotted line) and 1+2 phonon contributions are shown.

nificant. Also note that the NIS spectrum is dominated by hydrogen displacements because of the relatively large H neutron scattering cross section.

Figure 5 shows the dispersion curves of the low-energy modes along high-symmetry directions in the Brillouin zone. The high energy modes are quite dispersionless and thus not shown. It is interesting to point out that some of the modes have significant dispersion, such as those between 25-30 meV. This is surprising, considering the rigidity of the units (i.e., the $ZnO_4$ cluster and the BDC linker). We find that the dispersion comes from the points where these two rigid units are connected. This

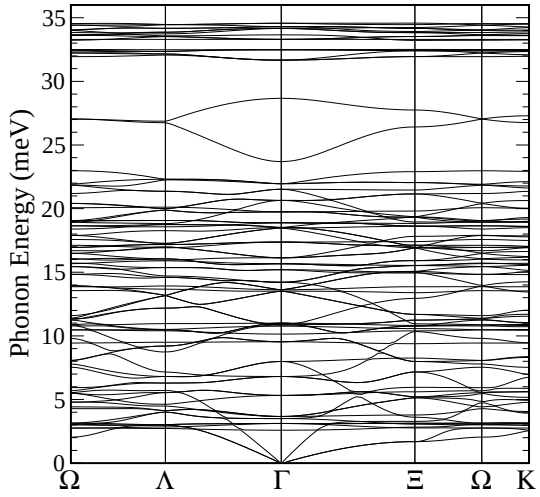


FIG. 5: Calculated phonon dispersion curves along high-symmetry directions in the Brillouin zone for MOF5. For clarity, only low energy (0-40 meV) portion is shown.

is also the reason for the very low shear modulus $c_{44}$. Another interesting result is the very low energy modes near 3 meV, which are quite flat. Some of these phonon modes will be discussed in detail below. Up to now, no phonon-dispersion measurement on MOF5 has been reported, partly due to the difficulty of growing a large single crystal needed for the experiment. We hope that in the near future, some of the phonon dispersions that we predict here can be experimentally confirmed.

We next discuss several interesting modes revealed by the phonon calculations. Animations of these phonon modes are available in Ref.[17] for direct visualization. The lowest energy mode ($A_{2g}$, 2.59 meV) is singly degenerate, with all $C_6H_4$ linkers twisting around the crystal axis direction. This mode is basically dispersionless (see Fig. 5) which is due to negligible interaction between two adjacent benzene linkers along the crystal axis. The second lowest energy mode ($T_{1g}$, 3.12 meV, 3-fold degenerate) can be described as two of three $C_6H_4$ linkers twisting around the two corresponding crystal axes. These two softest twisting modes imply that the bonds between the organic linkers and the metal clusters are the most unstable part of the MOF structure. The ∼0.53 meV energy difference between the two modes suggests a coupling of the twisting motions of the nearest-neighbor benzene linkers.

Since the energy of the twisting mode is very low, one may wonder if the benzene ring is free to rotate at high temperatures. This could have important consequences on the hydrogen absorption dynamics in MOF5. If the linker is rotated $90^o$, it could block the channels connecting the cubic cavities in MOF5 available for hydrogen storage. Motivated by these arguments, we have investigated the dynamics of the linker using quasielastic neutron scattering measurements[18]. However, we did not observe any free rotation of the linker at high tempera-

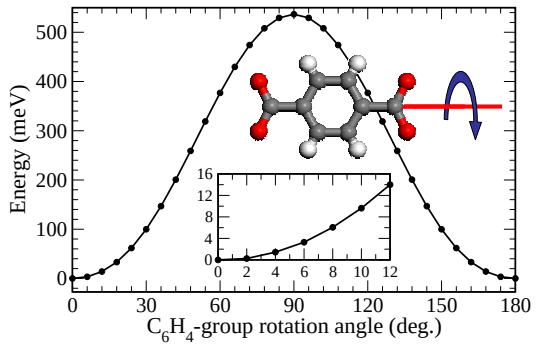


FIG. 6: (Color online) The variation of the total energy as one of the $C_6H_4$ groups (part of the BDC organic linker of MOF5) is twisted around the crystal axis direction. Note that the initial twisting does not cost much energy (see inset) although the energy barrier for the $180^o$ flipping (two-site jumping) of the $C_6H_4$ group is rather large (∼537 meV).

ture nor any evidence of the $\pi$-rotational jumps of the linker. These findings later became clear when we looked at the potential curve as the $C_6H_4$ linker is rotated. We performed total energy calculations as a function of the rotational angle of the benzene plane. For simplicity, we only twisted one of the six benzene rings in the primitive cell. The results are shown in Fig.6. The overall barrier is surprisingly large (∼537 meV), consistent with the quasielastic neutron scattering results. However, twisting for a few degrees only costs an energy of several meV (see the inset of Fig. 6), in agreement with the phonon modes being very soft. The third lowest energy mode (3.50 meV, $T_{2u}$, 3-fold degenerate) involves all $C_6H_4$ linkers translating along crystal axis $a$, $b$, and $c$. All other modes with E < 23 meV are various combinations of the motion of the $C_6H_4$ linker as a whole and the vibration of the $ZnO_4$ clusters. Two modes at slightly higher energy (23.69 meV, $A_{2u}$ and 28.67 meV, $A_{1g}$) are the breathing modes of the $ZnO_4$ cluster, with the clusters vibrating in the unit cell out-of-phase and in-phase, respectively. Most of other modes falling in the energy range of our NIS measurement are one of the twisting, stretching, breathing, bending and wagging motions of the benzene rings. They can be roughly divided into two groups. With E < ∼70 meV, the phonon modes are more dominated by the C displacements of the $C_6H_4$ linkers. The modes in the higher energy region are more dominated by H displacements.

The highest energy modes (380-385 meV, not covered by our NIS data) are totally dominated by the C-H covalent bond and all are associated with various C-H stretching modes of the $C_6H_4$ group.

In summary, we presented a detailed lattice dynamics study of MOF5 combining first-principles calculations and neutron inelastic scattering measurements. Our results indicated that MOFs are an interesting class of materials in terms of structural stability and dynamical properties. We identified the modes associated with the twisting of the linker to be the softest modes in the structure and therefore expected to be populated first with increasing temperature, eventually leading to structural instability. This is also consistent with the very small shear modulus $c_{44}$ that we have calculated. Despite the very low energy of the linker twisting modes, we found a very large energy barrier for the full rotation of the linker. We hope that our calculations will initiate further experiments to confirm our predictions. In particular, our results suggest that MOF5 is very close to structural instability, possibly leading to an interesting structural transformation under high pressure.

The authors thank Drs. T. J. Udovic and M. R. Hartman for technical help in the NIS data collection. We also acknowledge partial support from DOE under BES grant DE-FG02-98ER45701.

[1] M. Eddaoudi et al., Science **295**, 469 (2002).
[2] O. M. Yaghi et al., Nature **423**, 705 (2003).
[3] H. K. Chae et al., Nature **427**, 523 (2004)
[4] N. Ockwig, O. D. Friedrichs, M. O'Keeffe, O. M. Yaghi, Acc. Chem. Res. **38**, 176 (2005)
[5] S. Hamel, V. Timoshevskii, and Michel Cote, Phys. Rev. Lett. **95**, 146403 (2005)
[6] J. Rowsell, J. Eckert, OM Yaghi. J. Am. Chem. Soc. **127**, 14904 (2005)
[7] W. Zhou and T. Yildirim, in preparation
[8] S. Baroni, A. Dal Corso, S. de Gironcoli, and P. Giannozzi, http://www.pwscf.org.
[9] F. D. Murnaghan, Proc. Natl. Acad. Sci. U.S.A. **30**, 244 (1944).
[10] T. Yildirim and M. R. Hartman, Phys. Rev. Lett. **94**, 175501 (2005).
[11] M. J. Mehl, B. M. Klein, and D. A. Papaconstantopoulos, "First-Principles Calculation of Elastic Properties," Intermetallic Compounds: Principles and Applications, ed. J. H. Westbrook and R. L. Fleischer (London: John Wiley & Sons Ltd., 1994).
[12] O. Beckstein, J. E. Klepeis, G. L. W. Hart, and O. Pankratov, Phys. Rev. B **63**, 134112 (2001).
[13] M. Born and K. Huang, in Dynamical Theory of Crystal Lattices (Oxford University Press, Oxford,1985), p. 136–140.
[14] T. Yildirim, Chem. Phys. **261**, 205 (2000).
[15] T. J. Udovic, D. A. Neumann, J. Leão, and C. M. Brown, Nuclear Instruments and Methods in Phys. Research A **517**, 189 (2004).
[16] G. L. Squires, Introduction to the theory of thermal neutron scattering (Dover, New York, 1996).
[17] http://www.ncnr.nist.gov/staff/taner/h2
[18] M. Bee, Quasielastic Neutron Scattering (Hilger, Bristol, 1988).